**Supporting Information.**

# ZIF-derived "senbei"-like $Co_9S_8/CeO_2/Co$ heterostructural nitrogen-doped carbon nanosheets as bifunctional oxygen electrocatalyst for Zn-air batteries

*Yinqing Sun[a], Yi Guan[a], Xiaochao Wu[a], Wanqing Li*[a,b], Yongliang Li[a], Lingna Sun[a], Hongwei Mi[a], Qianling Zhang[a], Chuanxin He[a], Xiangzhong Ren*[a]*

[a] *College of Chemistry and Environmental Engineering, Shenzhen University, Shenzhen 518060, China*

[b] *Key Laboratory of Optoelectronic Devices and Systems of Ministry of Education and Guangdong Province, College of Physics and Optoelectronic Engineering, Shenzhen University, Shenzhen 518060, China*

*Corresponding author.

Xiangzhong Ren, Email: renxz@szu.edu.cn, Tel/Fax: +86-755-26558134

Wanqing Li, Email: liwanqing136@foxmail.com

## 1 Sample characterizations

The morphology and microstructure were characterized by field emission scanning electron microscopy (FESEM, JEOL JSM-7800F) and transmission electron microscopy (TEM, FEI Tecnai G2 F30). The EDS mapping was detected by field emission transmission electron microscope (TEM, JEOL JEM-F200). The phase existence and crystal plane were investigated by X-ray diffraction (XRD) on a PANalytical/Empyrean with Cu Kα radiation. Raman spectra were obtained using the Renishaw/INVIA REFLEX spectrometer. $N_2$ adsorption-desorption isotherms were measured by the BELSORP-max instrument. The specific surface area and pore size distribution were demonstrated by Brunauer-Emmett-Teller (BET) theory and nonlocal density functional theory (NLDFT), respectively. X-ray photoelectron spectroscopy (XPS) measurements were performed on a K-Alpha+ spectrometer equipped with a monochromic Al X-ray source.

## 2 Electrochemical measurement

### 2.1 Preparation of the working electrode

5 mg of the sample was dispersed into 1.5 mL of ethanol with 40 μL 5 wt% Nafion added, and the mixture was sonicated for 30 min. Afterwards, 15 μL of electrocatalyst ink was dropped on a glassy carbon RRDE disk (Φ=4 mm, $A_{disk}$=0.126 $cm^2$, $A_{ring}$=0.188 $cm^2$, inner/outer-ring diameter=5.0/7.0 mm) from BAS Inc. The loading of the catalyst is 0.398 mg $cm^{-2}$.

### 2.2 Electrochemical evaluations

All potential values are calibrated according to the reversible hydrogen electrode

(RHE). The electrochemical measurement was performed in a three-electrode system using Ag/AgCl (saturated KCl) as the reference electrode and Pt wire as the counter electrode, and all test are taken at the temperature of 25 °C. The linear sweep voltammogram (LSV) test was conducted at different speeds from 625 to 2025 rpm with a scan rate of 5 mV $s^{-1}$. The accelerated durability test was carried out in an $O_2$-saturated 0.1 M KOH solution with the scan rate of 100 mV $s^{-1}$ at a potential window of 0.2-1.0 V and 1.2-1.9 V for ORR and OER respectively. During the i-t stability test of ORR, 1mL $CH_3OH$ was introduced into the electrolyte to measure the anti-toxicity ability. Commercialized 20 wt% Pt/C (20 μg·$cm^{-2}$) and Ir/C (0.1 μg·$cm^{-2}$) were used as standard electrocatalysts for ORR and OER, respectively. The electrochemical double-layer capacitance ($C_{dl}$) of the electrocatalyst was measured by the CV test, and a potential range of 0.99-1.09 V was selected for capacitance measurement.

**2.3 Calculation of electron transfer number (n) and %$HO^{2-}$ for the oxygen reduction reaction**

The electron transfer number (n) can be determined using Koutecky–Levich (K–L) equations as given by:

$$\frac{1}{J} = \frac{1}{B\omega^{1/2}} + \frac{1}{J_K} \quad (1)$$

in which

$$B = 0.2nFC_0\ (D_0)^{2/3} v^{-1/6} \quad (2)$$

$$J_K = nFkC_0 \quad (3)$$

where J is the measured current density, JK is the kinetic limiting current density, ω is the angular velocity of the disk (ω = 2πN, where N is the linear rotation speed),

and n is the overall number of electrons transferred in oxygen reduction. F is the Faraday constant (F = 96485 C $mol^{-1}$), $C_0$ is the bulk concentration of $O_2$, ν is the kinematic viscosity of the electrolyte, k is the electron transfer rate constant, and $D_0$ is the diffusion coefficient of $O_2$ in the electrolyte. The constant 0.2 is adopted when the rotation speed is expressed in rpm. In this paper, the electron transfer number is measured from the LSV plots at potentials of 0.3, 0.4 and 0.7 V.

The electron transfer number (n) and the corresponding peroxide yield ($HO^{2-}$ in alkaline solution) can also be determined on the basis of the disk and ring currents using the following equations:

$$n = 4 \times \frac{I_{disk}}{I_{disk} + I_{ring} / N} \quad (4)$$

$$peroxide\% = 100 \times \frac{2I_{ring} / N}{I_{disk} + I_{ring} / N} \quad (5)$$

where $I_{disk}$ and $I_{ring}$ are the Faraday disk and ring currents, respectively. N is the collection efficiency of the ring electrode, which is determined to be 0.43 here. The disk electrode was scanned at a rate of 5 mV $s^{-1}$, and the ring potential was constant at 0.5 V.

**2.4 Zinc-Air battery tests**

The performance of zinc-air batteries was evaluated in self-made batteries with the air cathode constructed by dispersing the electrocatalyst on 1.5 cm × 5 cm gas diffusion layer of 1.0 mg $cm^{-2}$ and the anode of Zinc plat. 6.0 M KOH mixed with 0.2 M $Zn(Ac)_2$ was used as an electrolyte. As a comparison, mechanical mixture of commercial Pt/C and Ir/C (mass ratio = 1:1) was used as a control group. The long-term charging ability

of the Zn-air battery was evaluated by constant current charge and discharge at a current density of 2 and 5 mA $cm^{-2}$, 20 minutes for (10 minutes for charging and 10 minutes for discharging). These constant current charge/discharge curves were recorded by LAND battery test station (CT2001A)

**Fig. S1.** The photo of precursor Ce.

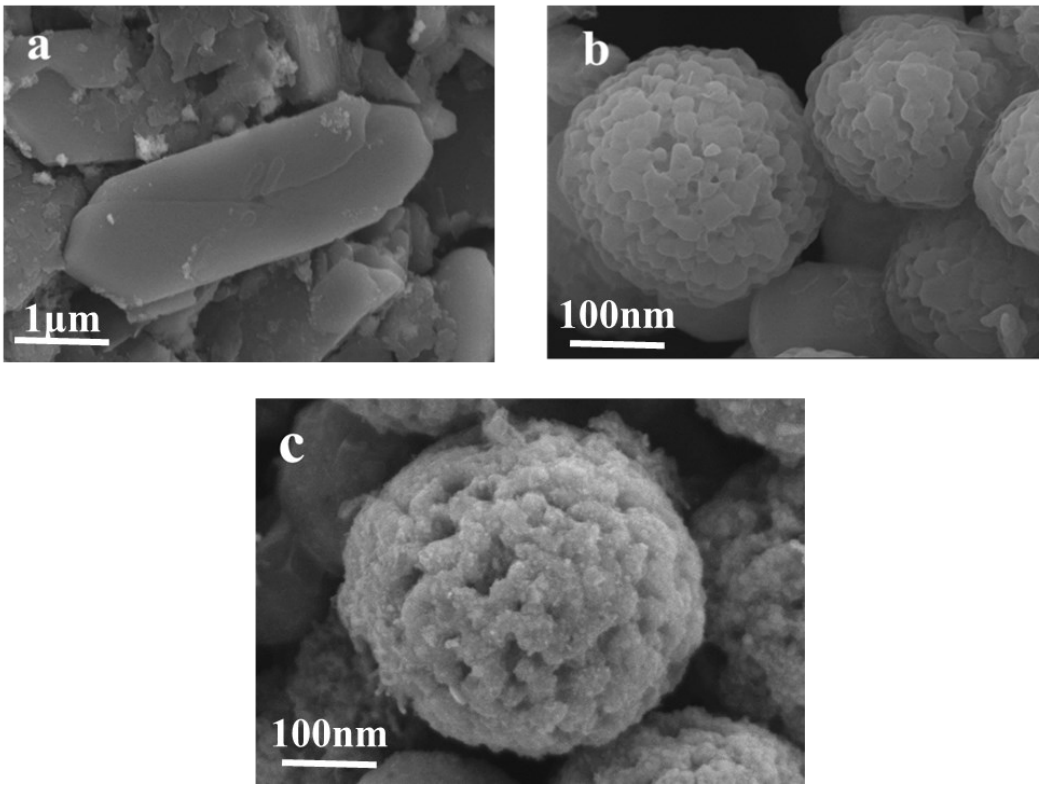


**Fig. S2.** SEM image of (a) Co/Ce-ZIF, (b) Co-ZIF and (c) $Co_9S_8$/Co-NC.

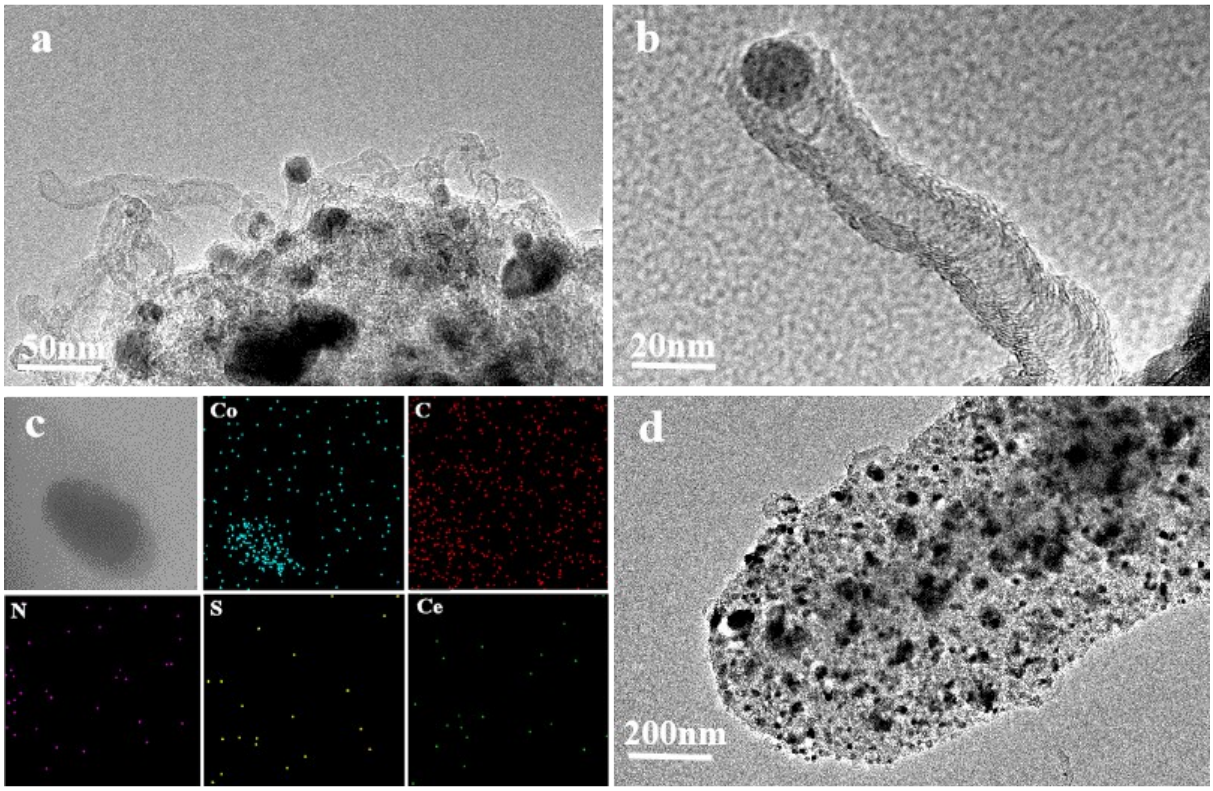


**Fig. S3.** TEM image of (a) the carbon nanotubes grown on the $Co_9S_8/CeO_2$/Co-NC nanosheets and (b) HRTEM image of the carbon nanotube with nanoparticle encapsulated on the top. (c) EDS element mapping images of the nanoparticle wrapped in the CNT. (d) TEM image of $Co_9S_8/CeO_2$/Co-NC obtained after sulfidation.

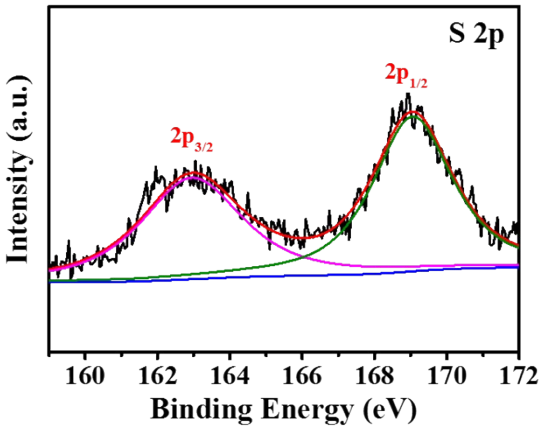


**Fig. S4.** S 2p spectrum of the $Co_9S_8$/Co-NC.

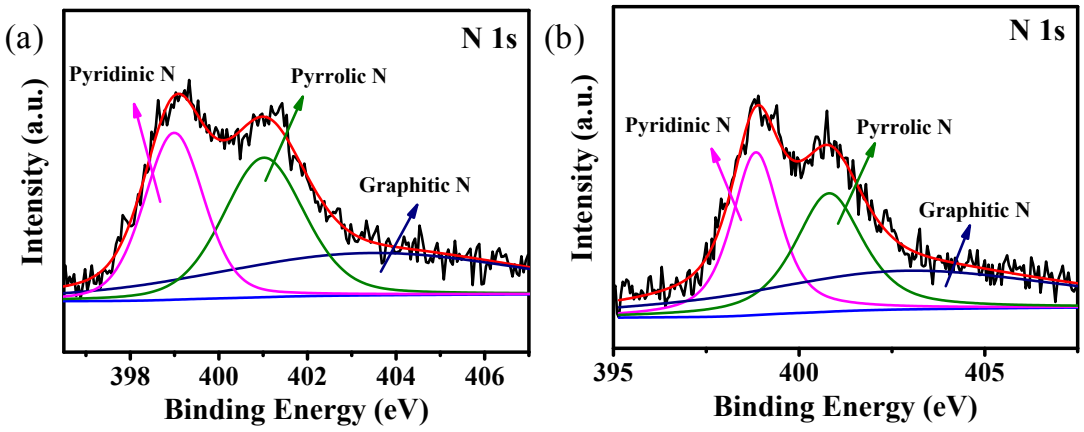


**Fig. S5.** N 1s spectra of the (a) $CeO_2$/Co-NC and (b) $Co_9S_8$/Co-NC.

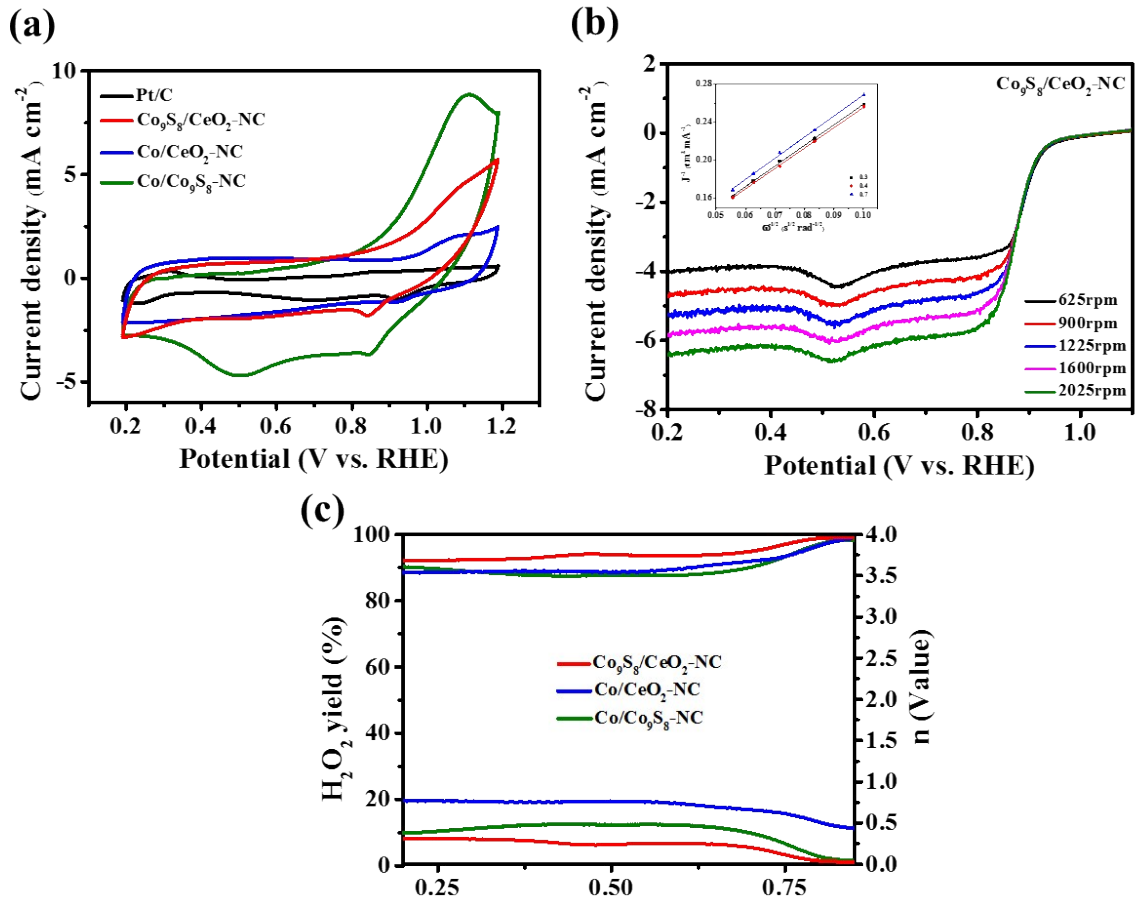


**Fig. S6.** (a) CV curves for Pt/C, $Co_9S_8/CeO_2$/Co-NC, $CeO_2$/Co-NC and $Co_9S_8$/Co-NC in $O_2$-saturated 0.1 M KOH solution in the potential window of 0.2-1.2 V at a scan rate of 5mV $s^{-1}$; (b) LSV curves of the $Co_9S_8/CeO_2$/Co-NC electrocatalyst at various rotation rate and the inset is the corresponding K-L plot; (c) The percentage of peroxide in the total oxygen reduction products and the number of electron transfers for the $Co_9S_8/CeO_2$/Co-NC, $CeO_2$/Co-NC and $Co_9S_8$/Co-NC electrodes.

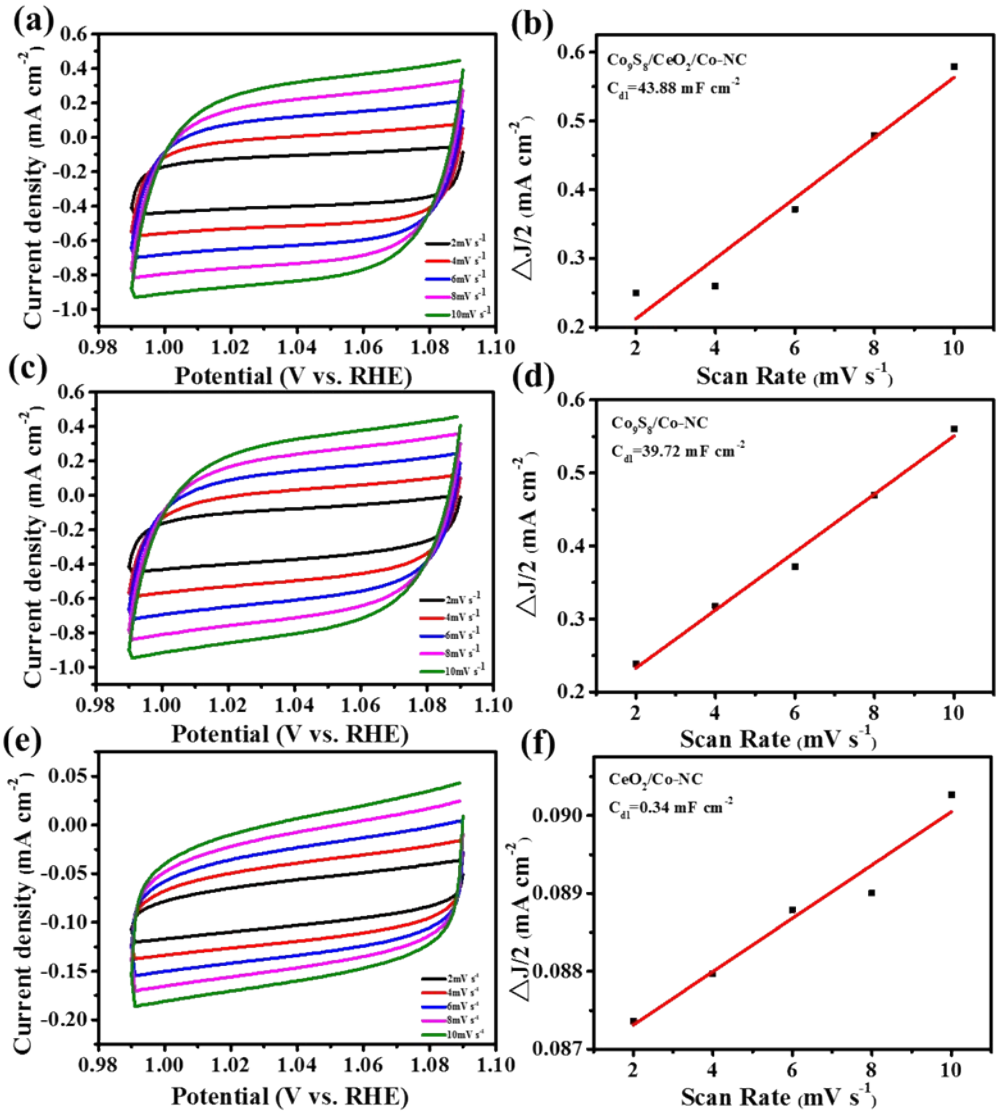


**Fig. S7.** Cyclic voltammograms in the region of 0.99-1.09 V vs. RHE at various scan rates and the corresponding linear fitting of the capacitive currents vs. scan rates to estimate the $C_{dl}$. (a) and (b) for $Co_9S_8/CeO_2$/Co-NC; (c) and (d) for $Co_9S_8$/Co-NC; (e) and (f) for $CeO_2$/Co-NC; the calculated $C_{dl}$ values are shown in the pictures.

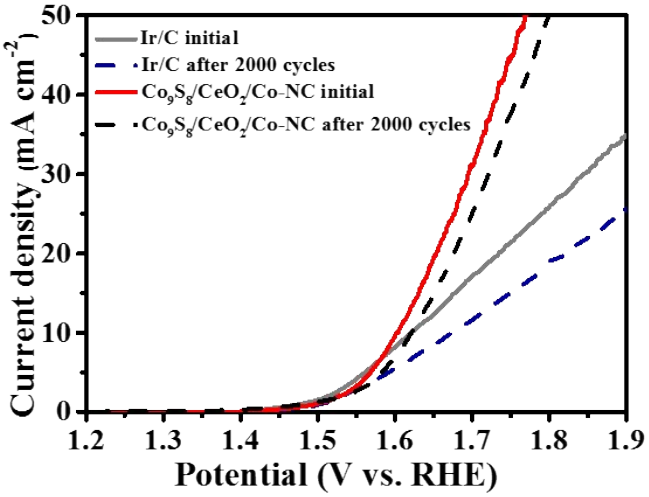


**Fig. S8.** LSV curves of Ir/C and $Co_9S_8/CeO_2$/Co-NC before and after 2000 CV cycles at a potential range of 0.2-1.2V versus RHE at a sweep speed of 100 mV $s^{-1}$.

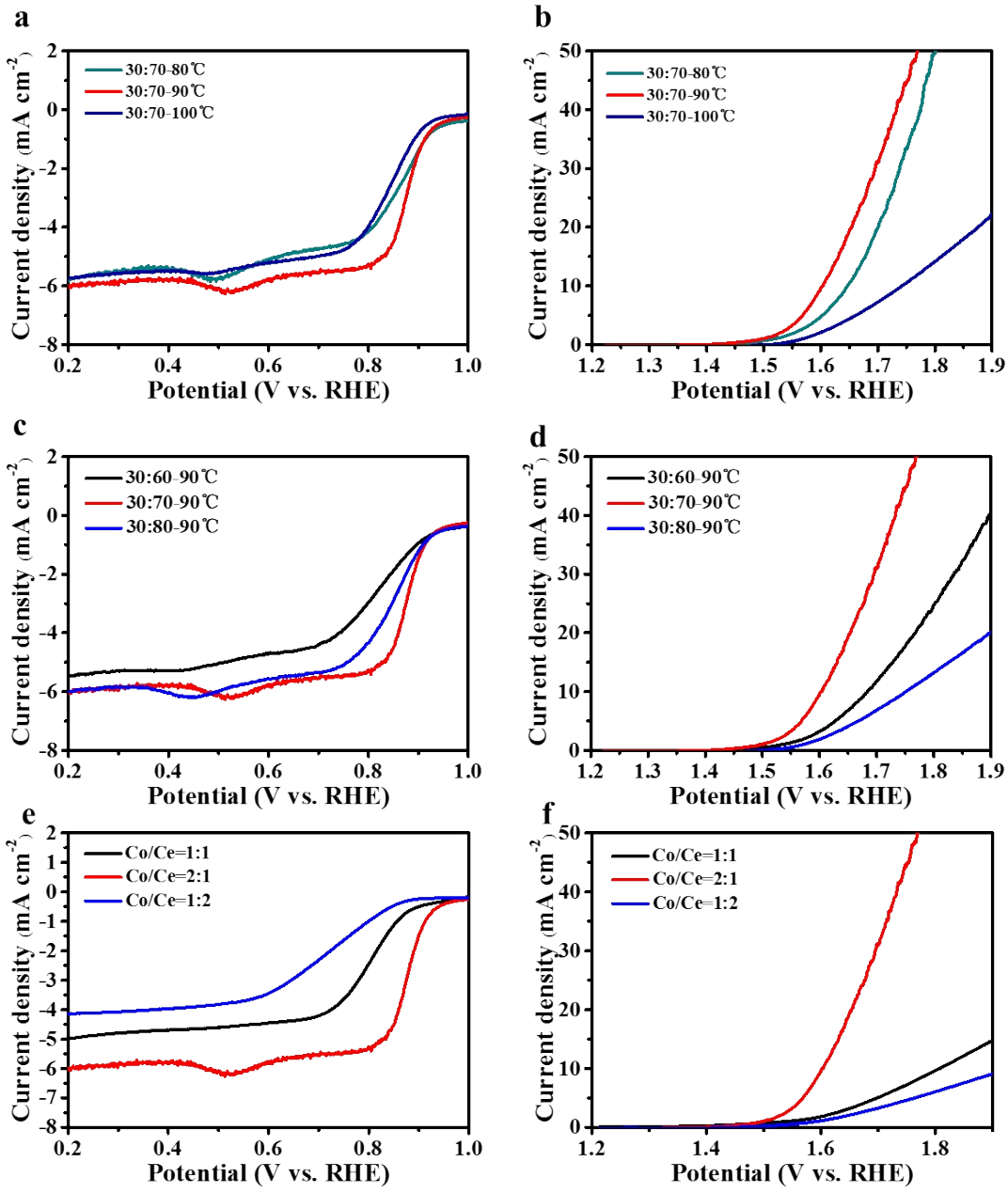


**Fig. S9.** LSV curves for the ORR and OER at 1600 rpm in 0.1 M KOH at a scan rate of 5 mV $s^{-1}$ of $Co_9S_8/CeO_2$/Co-NC obtained (a,b) under different mass ratio at the oil bath heating temperature of 90°C ;(c,d) under different oil bath heating temperature when the mass ratio is the same and (e,f) under different input molar ratios of Co/Ce.

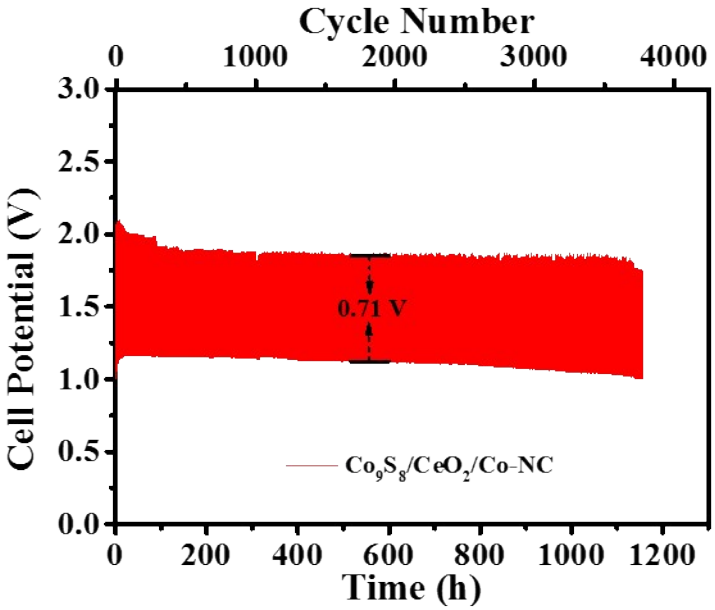


**Fig. S10.** Galvanostatic cycling stability tests of the Zn–air battery with the $Co_9S_8/CeO_2$/Co-NC electrocatalysts at a current density of 2 mA $cm^{-2}$.

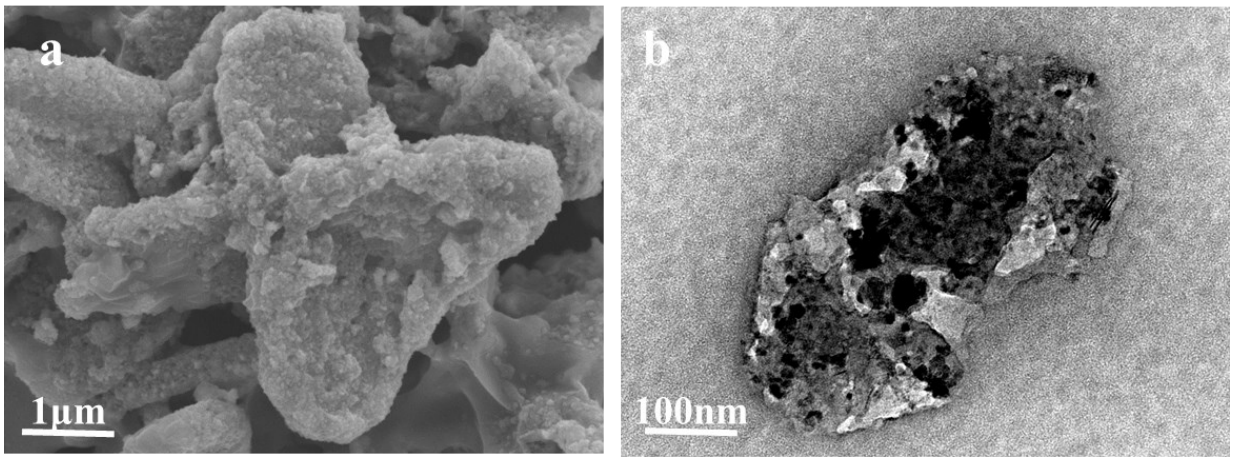


**Fig. S11.** (a) SEM and (b) TEM images of $Co_9S_8/CeO_2$/Co-NC after the charge/discharge cycling test.

**Table S1.** XPS results analysis for the samples prepared under different input molar ratios of Co/Ce (at. %).

| Sample | Co/Ce (input molar ratio) | Co2p (at.%) | Ce3d (at.%) | S2p (at.%) | N1s (at.%) | O1s (at.%) | C1s (at.%) |
|---|---|---|---|---|---|---|---|
| $Co_9S_8/CeO_2$ /Co-NC | 1:1 | 4.23 | 1.69 | 4.21 | 3.41 | 17.04 | 69.41 |
| | **2:1** | **5.16** | **1.63** | **4.57** | **3.35** | **14.97** | **70.32** |
| | 1:2 | 4.31 | 2.96 | 3.71 | 3.00 | 17.51 | 68.51 |

**Table S2.** Bifunctional activities for ORR and OER of the samples synthesized under different mass ratios when the oil bath heating temperature is 90°C.

| Electrocatalyst | Mass ratio (precursor:TAA) | $E_{j=10}$ (V) | $E_{1/2}$(V) | $E_{onset}$(V) | $\Delta E(E_{j=10}-E_{1/2})$ (V) |
|---|---|---|---|---|---|
| $Co_9S_8/CeO_2/Co$ -NC | 30:60 | 1.68 | 0.80 | 0.943 | 0.88 |
| | **30:70** | **1.60** | **0.875** | **0.946** | **0.725** |
| | 30:80 | 1.75 | 0.847 | 0.945 | 0.903 |

**Table S3.** Bifunctional activities for ORR and OER of the samples synthesized under different oil bath heating temperature when the mass ratios is 30:70.

| Electrocatalyst | Oil bath heating temperature | $E_{j=10}$ (V) | $E_{1/2}$(V) | $E_{onset}$(V) | $\Delta E(E_{j=10}-E_{1/2})$ (V) |
|---|---|---|---|---|---|
| $Co_9S_8/CeO_2/Co$-NC | 80°C | 1.64 | 0.840 | 0.945 | 0.80 |
| | **90°C** | **1.60** | **0.875** | **0.946** | **0.725** |
| | 100°C | 1.73 | 0.823 | 0.925 | 0.907 |

**Table S4.** Bifunctional activities for ORR and OER of the samples synthesized under different input molar ratios of Co/Ce.

| Electrocatalyst | Co/Ce (input molar ratio) | $E_{j=10}$ (V) | $E_{1/2}$(V) | $E_{onset}$(V) | $\Delta E(E_{j=10}-E_{1/2})$ (V) |
|---|---|---|---|---|---|
| $Co_9S_8/CeO_2/Co$-NC | 1:1 | 1.80 | 0.81 | 0.885 | 0.99 |
| | **2:1** | **1.60** | **0.875** | **0.946** | **0.725** |
| | 1:2 | / | 0.735 | 0.878 | / |

**Table S5.** Bifunctional activities for ORR and OER of as-prepared catalysts.

| **Electrocatalyst** | **$E_{j=10}$ (V)** | **$E_{1/2}$(V)** | **$E_{onset}$(V)** | **$\Delta E(E_{j=10}-E_{1/2})$ (V)** |
|---|---|---|---|---|
| **$Co_9S_8/CeO_2$/Co-NC** | **1.60** | **0.875** | **0.946** | **0.725** |
| Co/$CeO_2$-NC | 1.83 | 0.83 | 0.917 | 1.00 |
| Co/$Co_9S_8$ -NC | 1.64 | 0.85 | 0.946 | 0.79 |
| Pt/C-Ir/C | 1.62 (for Ir/C) | 0.85 (for Pt/C) | 1.00 (for Pt/C) | 0.77 |

**Table S6**. The catalytic performance of various Co or/and Ce-based electrocatalysts from literatures.

| Electrocatalyst | ORR | OER | | ΔE | Literature |
|---|---|---|---|---|---|
| | $E_{onset}$ (V) | $E_{1/2}$ (V) | $E_{j=10}$ (V) | ($E_{j=10}$-$E_{1/2}$) (V) | |
| $Co_9S_8/CeO_2$/Co-NC | **0.946** | **0.875** | **1.60** | **0.725** | **This work** |
| $CoIn_2S_4$/S-rGO | 0.93 | 0.82 | 1.60 | 0.78 | [1] |
| IOSHs-NSC-$Co_9S_8$ | 0.92 | 0.82 | 1.64 | 0.82 | [2] |
| $CoS_x$@PCN/rGO | 0.89 | 0.78 | 1.57 | 0.79 | [3] |
| Ce-$LaCoO_3$(5.6 %) | 0.78* | 0.72 | 1.68 | 0.96 | [4] |
| $Co_9S_8$-NSHPCNF | 0.88* | 0.82 | 1.58 | 0.76 | [5] |
| N-$Co_9S_8$/G | 0.941 | 0.78* | 1.639 | 0.859 | [6] |
| $CeO_2$@NC-900 | 0.905 | 0.854 | 1.643 | 0.789 | [7] |
| Co-C@$Co_9S_8$ DSNCs | 0.96 | 0.83 | / | / | [8] |
| $Co_2P$/CoN-in-NCNTs | 0.96 | 0.85 | 1.65 | 0.80 | [9] |
| $CeO_2$-Co-NC | 0.922 | 0.797 | / | / | [10] |
| Ce-NiO-E | / | / | 1.612 | / | [11] |
| $Co_9S_8$(600)/N,S-GO | 0.95 | 0.75 | 1.63 | 0.88 | [12] |
| Co-$CNNs_{-0.7}$ | 0.875 | 0.803 | 1.67 | 0.867 | [13] |

* Not mentioned in the literatures but derived from the LSV curves.

**Table S7.** The survey of the performance of rechargeable Zn-air batteries with various electrocatalysts.

| Electrocatalyst | Peak power density (mW $cm^{-2}$) | Stability | Literature |
|---|---|---|---|
| $Co_9S_8/CeO_2$/Co-NC | **168** | **2,226 cycles of 668 h at 5 mA $cm^{-2}$** | **This work** |
| $CoIn_2S_4$/S-rGO | 133 | 150 cycles of 50 h at 10 mA $cm^{-2}$ | [1] |
| $CoS_x$@PCN/rGO | N/A | 394 cycles of 43.8 h at 50 mA $cm^{-2}$ | [3] |
| Ce-$LaCoO_3$(5.6 %) | 60 | 160 h at 2 mA $cm^{-2}$ | [4] |
| $Co_9S_8$-NSHPCNF | 113 | 1000 cycles of 166 h at 2 mA $cm^{-2}$ | [5] |
| $CeO_2$@NC-900 | 118.2 | 140 h at 5 mA $cm^{-2}$ | [7] |
| $Co_2P$/CoN-in-NCNTs | 194.6 | 96 h at 5 mA $cm^{-2}$ | [9] |
| Co-$CNNs_{-0.7}$ | 85.3 | 1000 cycles of 183 h at 10 mA $cm^{-2}$ | [13] |
| Co-N-CNTs | 101 | 130 cycles of 15 h at 2 $mA^{-2}$ | [14] |

## REFERENCES


1. G. Fu, J. Wang, Y. Chen, Y. Liu, Y. Tang, J. B. Goodenough and J.-M. Lee, *Adv. Energy Mater.,* 2018**, 8**, 1802263.
2. K. Tang, C. Yuan, Y. Xiong, H. Hu and M. Wu, *Appl. Catal. B-Environ.,* 2020, **260**, 118209.
3. W. Niu, Z. Li, K. Marcus, L. Zhou, Y. Li, R. Ye, K. Liang and Y. Yang, *Adv. Energy Mater.,* 2018, **8**, 1701642.
4. J. Qian, T. Wang, Z. Zhang, Y. Liu, J. Li and D. Gao, *Nano Energy,* 2020, **74**, 104948.
5. W. Peng, Y. Wang, X. Yang, L. Mao, J. Jin, S. Yang, K. Fu and G. Li, *Appl. Catal. B-Environ.,* 2020, **268**, 118437.
6. S. Dou, L. Tao, J. Huo, S. Wang and L. Dai, *Energy Environ. Sci.,* 2016, **9**, 1320-1326.
7. Y. Kang, W. Wang, J. Li, Y. Mi, H. Gong and Z. Lei, *J. Colloid Interface Sci.,* 2020, **578**, 796-804.
8. H. Hu, L. Han, M. Yu, Z. Wang and X. W. Lou, *Energy Environ. Sci.,* 2016, **9**, 107-111.
9. Y. Guo, P. Yuan, J. Zhang, H. Xia, F. Cheng, M. Zhou, J. Li, Y. Qiao, S. Mu and Q. Xu, *Adv. Funct. Mater.,* 2018, **28**, 1805641.
10. L. Lv, D. Zha, Y. Ruan, Z. Li, X. Ao, J. Zheng, J. Jiang, H. M. Chen, W.-H. Chiang, J. Chen and C. Wang, *ACS Nano,* 2018, **12**, 3042-3051.
11. W. Gao, Z. Xia, F. Cao, J. C. Ho, Z. Jiang and Y. Qu, *Adv. Funct. Mater.,* 2018, **28**, 1706056.
12. P. Ganesan, M. Prabu, J. Sanetuntikul and S. Shanmugam, *ACS Catal*., 2015, **5**, 3625-3637.
13. W.-J. Niu, J.-Z. He, Y.-P. Wang, Q.-Q. Sun, W.-W. Liu, L.-Y. Zhang, M.-C. Liu, M.-J. Liu and Y.-L. Chueh, *Nanoscale,* 2020, **12**, 19644-19654.
14. T. Wang, Z. Kou, S. Mu, J. Liu, D. He, I. S. Amiinu, W. Meng, K. Zhou, Z. Luo, S. Chaemchuen and F. Verpoort, *Adv. Funct. Mater.,* 2018, **28**, 1705048.